On Constitutive Models for the Momentum Transfer to Particles in Fluid-Dominated Two-Phase Flows

Yan Cui, Jure Ravnik, Matjaž Hriberšek, Paul Steinmann

Abstract This contribution deals with fluid flow-particle interactions in fluid dominated two phase flows. Spherical as well as non-spherical particles in form of prolate ellipsoids are considered. In the case of ellipsoids, the hydrodynamic drag force model based on the Brenner-type resistance tensor is applied. As high shear flow regions are frequently encountered in complex flow patterns, special attention is devoted to the extension of established shear lift models, that are only valid for special cases of shear flows, to a general shear lift model based on permutations of the lift tensor, originally derived by Harper and Chang. A generalized lift vector, valid for ellipsoidal particles, is derived and implemented for the computation of the lift force in general shear flows. The derived generalized shear lift force model is validated against other numerical models for ellipsoids in Couette flow, and its influence on the translational motion of ellipsoidal particles in a three-dimensional lid-driven cavity flow is studied. The computational results confirm the correctness of the proposed generalized shear lift model.

Yan Cui
University of Erlangen-Nuremberg, Chair of Applied Mechanics, Egerlandstr. 5, D-91058 Erlangen, Germany e-mail: yan.cui@fau.de

Jure Ravnik
University of Maribor, Faculty of Mechanical Engineering, Smetanova 17, SI-2000, Maribor, Slovenia e-mail: jure.ravnik@um.si

Matjaž Hriberšek
University of Maribor, Faculty of Mechanical Engineering, Smetanova 17, SI-2000, Maribor, Slovenia e-mail: matjaz.hribersek@um.si

Paul Steinmann
University of Erlangen-Nuremberg, Chair of Applied Mechanics, Egerlandstr. 5, D-91058 Erlangen, Germany e-mail: paul.steinmann@fau.de

1 Introduction

Fluid flows with dispersed solid particles are increasingly important in several fields of sciences, e.g. life sciences, natural sciences, medical sciences and engineering sciences. Processing of suspensions with fibres in the pulp industry [18], regulating heat transfer by use of particles with favorable thermal properties [15], magnetic separation of particles from the matrix fluid [21], [31], and waste water treatment [14] are only a few of many applications. Dispersed flows consist of particles (drops, bubbles, solids) that move in a continuous phase (air, water). Particles interact with the fluid flow, i.e. in general, they exchange mass, linear and angular momentum, and energy. Among the interactions that predominantly influence a particle trajectory, the linear momentum exchange is typically the most important one. However, in cases of high shear flow fields and/or rotating particles, angular momentum can also play an important role and can in general not be neglected.

The influence of the particles on the fluid flow and the collisions between particles cannot be ignored. However, in the case of dilute suspensions we may reasonably ignore particle-particle interactions and limit our considerations to the particle-fluid system. This leads to the fundamental theory of non-colloidal suspensions, which aims to provide reduced scale models for the two-way coupling between particles and the fluid flows [4]. Also, in cases of small particles (micro and nano sized) modelling of particle-fluid interactions is unavoidable, as one can not afford to fully resolve flow structures in the vicinity of the particles. In order to develop accurate computational tools for the particle-fluid interaction, one needs to implement the appropriate constitutive models for the interaction of the two phases.

2 Particle-fluid interaction in fluid dominated flows

In the case of solid particles or micro sized bubbles and drops the shape of a particle is not affected by the flow field, therefore the particles can be considered to be rigid particles, immersed in the fluid phase. As the flow field is typically described in the Eulerian frame of reference, the relative motion of the particulate phase with respect to the fluid phase favours the implementation of the Lagrangian frame of reference for the computation of the particle dynamics. In this case, the action of the fluid flow on the dispersed phase can be accounted for by the well established Lagrangian particle tracking method. Here the particle position is obtained by solving additional equations for the particle kinematics (relation between the configurational variables and their velocities) and the particle dynamics (balances of momenta) [20].

In the case of dilute suspensions, the effect of the dispersed phase on the fluid phase is weak, establishing conditions where only the influence of the fluid flow on the dispersed particles needs to be accounted for, i.e. the one-way coupling interaction is governing the motion of particles. In this case, the computational framework for the particle-fluid interaction can be split subsequently into the computation of

the viscous fluid flow field, and the computation of the fluid flow's momentum exchange with the particles.

2.1 Viscous fluid flow

The computation of the numerical solution is predominantly performed in the Eulerian framework, where the flow field is typically described in terms of velocity and pressure fields. For fluid flow, the total change of a flow quantity in the control volume is due to the interaction with the surroundings of the control volume, i.e. due to surface and volumetric effects. Considering the net mass balance in a control volume leads to the continuity equation

$$\frac{\partial \rho_f}{\partial t} + \nabla \cdot [\rho_f \mathbf{u}] = 0, \tag{1}$$

where ρ_f is the fluid density and $\mathbf{u}$ is the fluid velocity. The continuity equation simplifies to $\nabla \cdot \mathbf{u} = 0$ for incompressible fluids.

Considering transport of momentum in a incompressible Newtonian fluid leads to the following momentum conservation equation

$$\frac{\partial \mathbf{u}}{\partial t} + [\mathbf{u} \cdot \nabla]\mathbf{u} = \mathbf{f}_f - \frac{1}{\rho_f}\nabla p + \nu \nabla^2 \mathbf{u}, \tag{2}$$

where ν is the fluid kinematic viscosity, p is the fluid pressure and $\mathbf{f}_f$ are volumetric source terms and fluid-particle interaction momentum exchange terms.

The evaluation of the translational momentum exchange between particles and fluid depends mainly on the data of the velocity field, whereas in the case of rotational momentum exchange (angular momentum, moment of momentum) it is essentially based on the vorticity field. As in the case of high shear flows there is also a strong influence of the vorticity field on the translational momentum exchange, the detailed information on the vorticity field,

$$\mathbf{w} = \nabla \times \mathbf{u} \tag{3}$$

being the curl of the velocity field, is also needed. The accuracy of the particle tracking scheme thus depends on the accurate calculation of velocity and vorticity fields. In the case of fluid dominated two-phase flows the contribution of the momentum exchange term $\mathbf{f}_f$ due to particle-fluid interactions is zero.

2.2 Particle dynamics

The trajectory of a particle is a result of its interaction with the fluid flow, which in fluid dominated flows determines its translational and angular velocity. In the case of small particles, typically in the micro and sub-micro range, the particles behave like rigid bodies, i.e. the deformation of a particle can be neglected. In order to determine the trajectory, particle transport is computed in the Lagrangian framework by particle tracking. Local values of velocity, vorticity and pressure in the fluid phase and their difference to the state of the particle determine transport phenomena between the dispersed and the fluid phase.

The particle linear momentum conservation equation is

$$\frac{d}{dt}(m_p\mathbf{v}) = m_p\frac{d\mathbf{v}}{dt} = m_p\mathbf{g}+\mathbf{F} \tag{4}$$

where m_p is the mass of the particle, $\mathbf{v}$ is the particle velocity, $\mathbf{g}$ is the gravity acceleration and $\mathbf{F}$ is the fluid force acting on the particle. The particle angular momentum conservation is

$$\frac{d}{dt}(\mathbf{I}_p\cdot\boldsymbol{\omega}) = \mathbf{I}_p\cdot\frac{d\boldsymbol{\omega}}{dt}+\boldsymbol{\omega}\times[\mathbf{I}_p\cdot\boldsymbol{\omega}] = \mathbf{T} \tag{5}$$

where $\mathbf{I}_p$ is the particle moment of inertia tensor, $\boldsymbol{\omega}$ is the particle angular velocity and $\mathbf{T}$ is the torque acting on the particle. Equations (4) and (5) enable determination of the change of velocities, which can then be applied to determine the new translational and angular positions of the particle by solving the kinematics equations. Translational kinematics is expressed using the particle barycentre position vector $\mathbf{r}$ as:

$$\frac{d\mathbf{r}}{dt} = \mathbf{v}. \tag{6}$$

In order to avoid singularity issues associated with the use of Euler angles rotational kinematics is usually expressed in terms of the time evolution of the Euler parameters [e_0, e_1, e_2, e_3]. The time evolution of the Euler parameters is connected to particle angular velocity expressed in the particle frame of reference.

2.3 Momentum transfer in particle-fluid interaction

The differences in velocity of the particle and the fluid velocity in the vicinity of the particle give rise to linear momentum exchange and in the case of angular velocity to angular momentum exchange. In fluid dominated flows,the fluid affects the trajectory of the particle but the particle doesn't influence the fluid flow, i.e. one-way coupling. In the ideal case, the resolved stresses on the surface of the particle are the only information needed to determine the impact of the flow on the particle dynamics.

2.3.1 Direct coupling

In fluid dominated flows, correct and accurate determination of the transfer of linear and angular momentum from the fluid to the rigid body presents the main modelling task. For direct coupling, one simultaneously integrates the Navier-Stokes equations, governing the fluid motion, and the equations of the rigid body motion, governing the motion of particles.

The linear momentum transfer from the fluid to the particle is encapsulated in the fluid force $\mathbf{F}$, acting on the particle. It is the integral over the particle surface of the traction $\sigma \cdot \mathbf{n}$ exerted from the fluid onto the particle surface Γ_p

$$\mathbf{F} = \int_{\Gamma_p} \sigma \cdot \mathbf{n} d\Gamma_p = \int_{\Gamma_p} \left[-p\mathbf{n} + \rho_f \nu \left[\nabla \mathbf{u} + \nabla \mathbf{u}^T \right] \cdot \mathbf{n} \right] d\Gamma_p \tag{7}$$

with $\mathbf{n}$ the normal particle surface vector.

The angular momentum transfer from the fluid to the particle is encapsulated in the torque $\mathbf{T}$, acting on the particle. The torque is the integral of the moment of the traction vector. As the particle is embedded in the fluid, at the surface of the particle no-slip conditions are applied, i.e. the fluid velocity is the same as the velocity at the particle surface,

$$\mathbf{u} = \mathbf{v} + \omega \times \mathbf{r}_p, \tag{8}$$

where $\mathbf{r}_p$ is a vector originating at the particle barycentre and pointing towards particle surface. In the above equations, the body can have an arbitrary shape, discretized by a suitable surface mesh.

Although the direct coupling eliminates the need to introduce specific models for different phenomena in momentum transfer, it is extremely expensive in terms of computational cost, when particle sizes are very small or when there are large numbers of particles to be tracked. The flow domain in the vicinity of the particle, as well as the particle surface, need to be correctly discretized, and the movement of the particles requires changes to the computational grid to be made during computations. In order to avoid this problem dedicated interaction models are developed and predominantly used in numerical simulations.

2.3.2 Coupling by dedicated interaction models

As already stated, in the case of small particles (micro, nano-sized particles) a direct computation of fluid-particle interaction is practically not feasible, as flow and particle surface resolution demands would be computationally extremely expensive. In order to overcome this problem, simplified models for the computation of the particle dynamics in fluid flow have to be implemented.

If particles are considered with diameters much smaller than the length scales of the smallest flow structures, there is no need to directly resolve the particle surface, and the point particle approximation can be implemented. In this case, the flow do-

main does not include particles, the interaction with the particulate phase is merely included in the source term $\mathbf{f}_f$ in equation (2).

Since the particle is considered as a point particle, the physical models for the evaluation of forces (and torques) on the particle rely on the velocity and vorticity fields evaluated at the position of the particle. The overall action of the fluid flow on the particle, in direct coupling evaluated by solving equation (7), is now decomposed into specific phenomena described by different models. In the translational momentum balance for the dispersed phase this means that each specific phenomena is described by a force model, and all the forces are assumed to be linearly additive. In general, particles move due to the additive action of gravity, buoyancy, drag, pressure gradient and added mass forces.

In a shear flow, an additional force, the so-called Saffman lift force [23, 24, 28, 5], occurs, which acts perpendicular to the flow direction. Its magnitude and direction are related directly to the local value of the vorticity of the fluid, and it acts on both non-rotating and rotating particles. Moreover, particle rotation gives rise to additional forces, most notably the Magnus lift force, influencing the translational motion of a particle. When the particle is also rotating, the angular momentum equation must therefore additionally be solved in order to capture the effect of particle orientation and particle rotation.

In order to track the particle's translational and rotational motion the particle position, the particle velocity, the particle orientation and the angular velocity of the particle have to be advanced in time in each computational step.

Dynamics of translational motion

Maxey and Riley [19] considered the forces on a small rigid sphere in a nonuniform flow and derived a consistent approximation for the equation of motion. They treated forces in the undisturbed flow and the flow disturbance caused by the presence of the sphere, separately. Brenner [1] developed the drag expression for arbitrary particles. Neglecting the aerodynamic lift, time history effects, second-order terms and due to the small particle size, we may write

$$m_p \frac{d\mathbf{v}}{dt} = [m_p - m_f]\mathbf{g} + m_f \frac{D\mathbf{u}}{Dt} - \frac{1}{2} m_f \left[\frac{d\mathbf{v}}{dt} - \frac{d\mathbf{u}}{dt} \right] + \pi a \rho_f \nu \mathbf{K} \cdot [\mathbf{u} - \mathbf{v}] + \mathbf{F}. \quad (9)$$

where a is the semi-minor axis of ellipsoidal particles. The terms included in the equation are gravity, buoyancy, pressure gradient term, added mass term and drag (skin friction and form drag). Here, $d/dt = \partial/\partial t + [\mathbf{v} \cdot \nabla]$ stands for the time derivative following the particle, i.e. the material time derivative of the particle and $D/Dt = \partial/\partial t + [\mathbf{u} \cdot \nabla]$ denotes the time derivative following the fluid element, i.e. the material time derivative of the fluid. $\mathbf{K}$ is the resistance tensor in direct notation, its coefficient are typically expressed with respect to the Eulerian (inertial) frame of reference, and $\mathbf{F}$ now stands for additional forces, acting on a particle (e.g. lift force).

Let us now consider prolate ellipsoidal particles with semi-minor axis a and semi-major axis b. The aspect ratio of the ellipsoid is $\lambda = b/a$. The density of the particle is ρ_p and the mass of fluid occupying the same volume as the particle is denoted by m_f. The volume of the particle is $V_p = \frac{4}{3}\pi a^2 b = \frac{4}{3}\pi a^3 \lambda$ and its mass is related to its density as $m_p = \frac{4}{3}\pi a^3 \lambda \rho_p$.

Equation (9) is rewritten in non-dimensional form with u_0 and L being the characteristic fluid velocity scale and the characteristic problem length scale, respectively. With $\mathbf{u} \to \mathbf{u}/u_0$, $\mathbf{v} \to \mathbf{v}/u_0$ and $t \to t u_0/L$ this eventually leads to

$$\mathbf{a} = \frac{d\mathbf{v}}{dt} = \frac{A}{St}\left[\mathbf{v}_s + \frac{1}{6\lambda}\mathbf{K}\cdot[\mathbf{u}-\mathbf{v}]\right] + \frac{3}{2}R\frac{\partial \mathbf{u}}{\partial t} + R\left[[\mathbf{u}+\frac{1}{2}\mathbf{v}]\cdot\nabla\right]\mathbf{u} + \mathbf{f} \tag{10}$$

where $\mathbf{a}$ is the particle acceleration and the Stokes number St is defined as

$$St = \frac{2}{9}\frac{\rho_p}{\rho_f}\frac{a^2 u_0}{\nu L}, \tag{11}$$

the sedimentation velocity is

$$\mathbf{v}_s = \frac{2a^2}{9\nu u_0}\left[\frac{\rho_p}{\rho_f} - 1\right]\mathbf{g}, \tag{12}$$

and the parameters R and A are

$$R = \frac{\rho_f}{\rho_p + \frac{1}{2}\rho_f}, \qquad A = \frac{\rho_p}{\rho_p + \frac{1}{2}\rho_f}. \tag{13}$$

The ellipsoidal particle response time was introduced by Shapiro and Goldenberg [26] as

$$\tau_p = \frac{2}{9}\frac{\rho_p}{\rho_f}\frac{a^2}{\nu}\frac{\lambda \ln(\lambda + \sqrt{\lambda^2 - 1})}{\sqrt{\lambda^2 - 1}}, \tag{14}$$

Since the characteristic fluid time scale is $\tau_f = L/u_0$, we may write the ellipsoid particle Stokes number as

$$St_e = St\frac{\lambda \ln(\lambda + \sqrt{\lambda^2 - 1})}{\sqrt{\lambda^2 - 1}}. \tag{15}$$

The hydrodynamic drag force, i.e. the term $\pi a \rho_f \nu \mathbf{K}\cdot[\mathbf{u}-\mathbf{v}]$ in equation (9), acting on an ellipsoidal particle under Stokes flow conditions was derived by Brenner [2]. It introduces the resistance tensor, which may be evaluated in the particle frame of reference $[x', y', z']$. In the particle frame of reference, only diagonal components of the resistance tensor $\mathbf{K}$ are non-zero. They are a function of the particle aspect ratio and may be written as:

$$K'_{x'x'} = K'_{y'y'} = \frac{16[\lambda^2 - 1]^{3/2}}{[2\lambda^2 - 3]\ln(\lambda + \sqrt{\lambda^2 - 1}) + \lambda\sqrt{\lambda^2 - 1}} \tag{16}$$

$$K'_{z'z'} = \frac{8[\lambda^2-1]^{3/2}}{[2\lambda^2-1]\ln(\lambda+\sqrt{\lambda^2-1})-\lambda\sqrt{\lambda^2-1}} \tag{17}$$

In the spherical particle limit $\lim_{\lambda\to 1}[\mathbf{K}]'$, one has $6[\mathbf{I}]$, where $\mathbf{I}$ is the identity tensor.

In order to express the coefficients of the resistance tensor in terms of the inertial reference frame, they must be rotated with respect to the current orientation of the particle. The rotation matrix, $\mathbf{V}$, is used in the following way:

$$[\mathbf{K}] = [\mathbf{V}^T][\mathbf{K}]'[\mathbf{V}], \tag{18}$$

where $\mathbf{V}^T$ is the transpose (inverse) of the rotation matrix, and $[\mathbf{K}]$, $[\mathbf{K}]'$ denote the coefficients of $\mathbf{K}$ in the inertial and the particle rotational frame of reference.

Orientation in space may be parameterized by the Euler angles $[\varphi,\theta,\psi]$. However, when kinematic relations between the angles and angular velocity are set up, we observe (Fantoni [7]) that a singularity exists for $\theta = 0$ and $\theta = \pi$. To avoid this problem, we express the orientation and the kinematic relations in terms of the Euler parameters instead. The Euler parameters (Goldstein [11]) are linked by a constraint

$$e_0^2 + e_1^2 + e_2^2 + e_3^2 = 1. \tag{19}$$

In the inertia frame the rotation matrix written in terms of the Euler parameters reads

$$[\mathbf{V}] = \begin{bmatrix} e_0^2+e_1^2-e_2^2-e_3^2 & 2[e_1e_2+e_0e_3] & 2[e_1e_3-e_0e_2] \\ 2[e_1e_2-e_0e_3] & e_0^2-e_1^2+e_2^2-e_3^2 & 2[e_2e_3+e_0e_1] \\ 2[e_1e_3+e_0e_2] & 2[e_2e_3-e_0e_1] & e_0^2-e_1^2-e_2^2+e_3^2 \end{bmatrix} \tag{20}$$

Subjecting spherical particles to high shear velocity the transverse lift force has to be accounted for [5, 23, 24, 28]

$$\mathbf{F}_{SL} = 6.46\rho_f a^2\sqrt{\nu}\frac{1}{\sqrt{|\mathbf{w}|}}[[\mathbf{u}-\mathbf{v}]\times\mathbf{w}] \tag{21}$$

Equation (21) is the well known Saffman lift force, and was further extended by Harper and Chang [12], Hogg [13] and Fan and Ahmadi [6] for non-spherical particles.

In a general shear flow, there exist six shear flows in the non-diagonal components of the velocity gradient tensor $\mathbf{G}$ with coefficients $\partial u_i/\partial j$ $(i,j\in\{x,y,z\}$, $i\neq j)$:

$$[\mathbf{G}] = \begin{bmatrix} \frac{\partial u_x}{\partial x} & \frac{\partial u_x}{\partial y} & \frac{\partial u_x}{\partial z} \\ \frac{\partial u_y}{\partial x} & \frac{\partial u_y}{\partial y} & \frac{\partial u_y}{\partial z} \\ \frac{\partial u_z}{\partial x} & \frac{\partial u_z}{\partial y} & \frac{\partial u_z}{\partial z} \end{bmatrix} \tag{22}$$

In the case of linear shear flow, only one non-diagonal component of the velocity gradient tensor has a non-zero value. Harper and Chang [12] derived a lift force for arbitrary three-dimensional rigid bodies moving in a linear shear flow $\partial u_x/\partial z$ at low

Reynolds numbers as:

$$\mathbf{F}_{SL} = \frac{1}{\rho_f \nu^{3/2}} \frac{\partial u_x/\partial z}{|\partial u_x/\partial z|^{1/2}} \mathbf{D} \cdot \mathbf{L_{xz}} \cdot \mathbf{D} \cdot [\mathbf{u}^L - \mathbf{v}] \tag{23}$$

where $\mathbf{u}^L = [u_x, 0, 0]$ is the reference flow for the lift, and the Stokes drag $\mathbf{F}_{D,Stokes} = \mathbf{D} \cdot [\mathbf{u}^L - \mathbf{v}]$. The lift tensor, calculated by asymptotic methods, in a linear shear flow $\partial u_x/\partial z$ is found to be [12]

$$[\mathbf{L_{xz}}] = \begin{bmatrix} 0.0501 & 0 & 0.0329 \\ 0 & 0.0373 & 0 \\ 0.0182 & 0 & 0.0173 \end{bmatrix} \tag{24}$$

In the case of spherical particles $\mathbf{D} = 6\pi\rho_f \nu a \mathbf{I}$, equation (23) can be written as:

$$\mathbf{F}_{SL} = 36\pi^2 \rho_f a^2 \sqrt{\nu} \frac{\partial u_x/\partial z}{|\partial u_x/\partial z|^{1/2}} \mathbf{L_{xz}} \cdot [\mathbf{u}^L - \mathbf{v}] \tag{25}$$

In the case of ellipsoidal particles $\mathbf{D} = \pi a \rho_f \nu \mathbf{K}$, one can then write the shear lift force found by Harper and Chang [12] for an ellipsoidal particle in the linear shear flow $\partial u_x/\partial z$ as

$$\mathbf{F}_{SL} = \pi^2 \rho_f a^2 \sqrt{\nu} \frac{\partial u_x/\partial z}{|\partial u_x/\partial z|^{1/2}} \mathbf{K} \cdot \mathbf{L_{xz}} \cdot \mathbf{K} \cdot [\mathbf{u}^L - \mathbf{v}] \tag{26}$$

Fan and Ahmadi [6] proposed an expression for the lift force acting on an ellipsoid in a different linear shear flow $\partial u_x/\partial y$, which can be expressed as:

$$\mathbf{F}_{SL} = \pi^2 \rho_f a^2 \sqrt{\nu} \frac{\partial u_x/\partial y}{|\partial u_x/\partial y|^{1/2}} \mathbf{K} \cdot \mathbf{L_{xy}} \cdot \mathbf{K} \cdot [\mathbf{u}^L - \mathbf{v}] \tag{27}$$

where the lift tensor $\mathbf{L_{xy}}$, is a permuted version of $\mathbf{L_{xz}}$, is given by

$$[\mathbf{L_{xy}}] = \begin{bmatrix} 0.0501 & 0.0329 & 0 \\ 0.0182 & 0.0173 & 0 \\ 0 & 0 & 0.0373 \end{bmatrix} \tag{28}$$

However, the above models of shear lift force of non-spherical particles are only applicable to linear shear flows. In the following, we propose a new lift force model for arbitrary shear flow. This model was originally developed by Ravnik et al. [22] and is further extended on by the present study. A similar model has been presented by Feng and Kleinstreuer [8]. In case of arbitrary shear flow, six equations like (26) and (27) are needed to describe a general shear flow and six permutations of lift tensors exist as well,

$$[\mathbf{L_{xy}}] = \begin{bmatrix} A & B & 0 \\ D & E & 0 \\ 0 & 0 & C \end{bmatrix} \qquad [\mathbf{L_{xz}}] = \begin{bmatrix} A & 0 & B \\ 0 & C & 0 \\ D & 0 & E \end{bmatrix} \tag{29}$$

$$[\mathbf{L_{yx}}] = \begin{bmatrix} E & D & 0 \\ B & A & 0 \\ 0 & 0 & C \end{bmatrix} \qquad [\mathbf{L_{yz}}] = \begin{bmatrix} C & 0 & 0 \\ 0 & A & B \\ 0 & D & E \end{bmatrix} \tag{30}$$

$$[\mathbf{L_{zx}}] = \begin{bmatrix} E & 0 & D \\ 0 & C & 0 \\ B & 0 & A \end{bmatrix} \qquad [\mathbf{L_{zy}}] = \begin{bmatrix} C & 0 & 0 \\ 0 & E & D \\ 0 & B & A \end{bmatrix} \tag{31}$$

where

$$A = 0.0501, B = 0.0329, C = 0.0373, D = 0.0182, E = 0.0173. \tag{32}$$

In the following we propose a generalized lift vector $\mathbf{l}$, defined as

$$\begin{aligned}
[\mathbf{l}] = &\left[\frac{\partial u_x/\partial y}{|\partial u_x/\partial y|^{1/2}} \mathbf{K}\cdot\mathbf{L_{xy}}\cdot\mathbf{K} + \frac{\partial u_x/\partial z}{|\partial u_x/\partial z|^{1/2}} \mathbf{K}\cdot\mathbf{L_{xz}}\cdot\mathbf{K} \right] \cdot \begin{bmatrix} u_x - v_x \\ -v_y \\ -v_z \end{bmatrix} + \\
&\left[\frac{\partial u_y/\partial x}{|\partial u_y/\partial x|^{1/2}} \mathbf{K}\cdot\mathbf{L_{yx}}\cdot\mathbf{K} + \frac{\partial u_y/\partial z}{|\partial u_y/\partial z|^{1/2}} \mathbf{K}\cdot\mathbf{L_{yz}}\cdot\mathbf{K} \right] \cdot \begin{bmatrix} -v_x \\ u_y - v_y \\ -v_z \end{bmatrix} + \\
&\left[\frac{\partial u_z/\partial x}{|\partial u_z/\partial x|^{1/2}} \mathbf{K}\cdot\mathbf{L_{zx}}\cdot\mathbf{K} + \frac{\partial u_z/\partial y}{|\partial u_z/\partial y|^{1/2}} \mathbf{K}\cdot\mathbf{L_{zy}}\cdot\mathbf{K} \right] \cdot \begin{bmatrix} -v_x \\ -v_y \\ u_z - v_z \end{bmatrix}
\end{aligned} \tag{33}$$

The lift force on a particle in a general shear flow can then be expressed by

$$\mathbf{F}_{SL} = \pi^2 \rho_f a^2 \sqrt{\nu}\, \mathbf{l} \tag{34}$$

The underlying idea is quite simple, i.e. sum of six shear lift forces. For the limiting case of a spherical particle with $\lambda \to 1$ one can obtain $\mathbf{K}\cdot\mathbf{L_{ij}}\cdot\mathbf{K} = 36\,\mathbf{L_{ij}}$. It should be noted that the j-component lift force induced by the velocity difference in the i-direction as evaluated from equations (33) and (34) agrees with the result of Saffman (Eq. 21), i.e. $36\pi^2 D = 6.46$, which corresponds to the finding of Harper and Chang [12] and Fan and Ahmadi [6]. In order to prevent numerical errors under the condition that $\partial u_i/\partial j = 0$, it is suggested adding a small value, i.e. $1.0e{-}18$, to the root of the equation (33).

The lift tensor $\mathbf{L_{ij}}$ is applicable for any arbitrarily shaped 3D body [12] and is used to determine the shear lift force for an ellipsoidal particle by applying $\mathbf{K}\cdot\mathbf{L_{ij}}\cdot\mathbf{K}$. The orientation of the ellipsoid is taken into account by equation (18). Therefore, the generalized shear lift force is applicable for particles with ellipsoidal and fibre shapes at low Reynolds numbers.

Dynamics of rotational motion

The rotational motion of a nonspherical particle moving in a flow field is governed by

$$I_{x'}\frac{d\omega_{x'}}{dt} - \omega_{y'}\omega_{z'}[I_{y'} - I_{z'}] = T_{x'} \tag{35}$$

$$I_{y'}\frac{d\omega_{y'}}{dt} - \omega_{z'}\omega_{x'}[I_{z'} - I_{x'}] = T_{y'} \tag{36}$$

$$I_{z'}\frac{d\omega_{z'}}{dt} - \omega_{x'}\omega_{y'}[I_{x'} - I_{y'}] = T_{z'} \tag{37}$$

where $\omega_{x'}$, $\omega_{y'}$, $\omega_{z'}$ are the particle angular velocities with respect to the principal axes, $I_{x'}$, $I_{y'}$, $I_{z'}$ are the particle moments of inertia about the principal axes [x', y', z'], i.e. the principal components of the particle's inertia tensor, and $T_{x'}$, $T_{y'}$, $T_{z'}$ are the hydrodynamic torques acting on the particle with respect to the principal axes. The rotational motion of the particle in equations (35) - (37) is stated in the particle reference frame.

The moments of inertia for an ellipsoid are

$$I_{x'} = I_{y'} = \frac{[1+\lambda^2]a^2}{5}m_p = \frac{4\pi}{15}\lambda[\lambda^2+1]a^5\rho_p \tag{38}$$

$$I_{z'} = \frac{2a^2}{5}m_p = \frac{8\pi}{15}\lambda a^5\rho_p \tag{39}$$

The flow near a small particle may be approximated as a linear shear flow. The hydrodynamic torque acting on an ellipsoidal particle suspended in a linear shear flow was derived by Jeffery [16]. In the particle reference frame, we have

$$T_{x'} = \frac{16\pi\rho_f\nu a^3\lambda}{3[\beta_0+\lambda^2\gamma_0]}\left[[1-\lambda^2]f' + [1+\lambda^2][\xi' - \omega_{x'}]\right] \tag{40}$$

$$T_{y'} = \frac{16\pi\rho_f\nu a^3\lambda}{3[\alpha_0+\lambda^2\gamma_0]}\left[[\lambda^2-1]g' + [1+\lambda^2][\eta' - \omega_{y'}]\right] \tag{41}$$

$$T_{z'} = \frac{32\pi\rho_f\nu a^3\lambda}{3[\alpha_0+\beta_0]}[\chi' - \omega_{z'}] \tag{42}$$

where f', g' are elements of the deformation rate tensor $\mathbf{D} := \mathbf{G}^{sym}$ and ξ', η' and χ' are elements of the spin tensor $\mathbf{W} := \mathbf{G}^{skw}$ with $\mathbf{w}$ the axial vector of $\mathbf{W}$, defined as

$$f' = \frac{1}{2}\left[\frac{\partial u_{z'}}{\partial y'} + \frac{\partial u_{y'}}{\partial z'}\right], \qquad g' = \frac{1}{2}\left[\frac{\partial u_{x'}}{\partial z'} + \frac{\partial u_{z'}}{\partial x'}\right] \tag{43}$$

$$\xi' = \frac{1}{2}\left[\frac{\partial u_{z'}}{\partial y'} - \frac{\partial u_{y'}}{\partial z'}\right], \quad \eta' = \frac{1}{2}\left[\frac{\partial u_{x'}}{\partial z'} - \frac{\partial u_{z'}}{\partial x'}\right], \quad \chi' = \frac{1}{2}\left[\frac{\partial u_{x'}}{\partial y'} - \frac{\partial u_{y'}}{\partial x'}\right] \tag{44}$$

In order to evaluate these terms, the velocity gradient tensor $\mathbf{G}$ must be rotated into the particle frame of reference using the rotation matrix as

$$[\mathbf{G}]' = [\mathbf{V}]\,[\mathbf{G}]\,[\mathbf{V}^T] \tag{45}$$

The nondimensional coefficients α_0, β_0 and γ_0 were defined by Gallily and Cohen [10] as

$$\alpha_0 = \beta_0 = \frac{\lambda^2}{\lambda^2-1} + \frac{\lambda}{2[\lambda^2-1]^{3/2}} \ln\left(\frac{\lambda-\sqrt{\lambda^2-1}}{\lambda+\sqrt{\lambda^2-1}}\right) \tag{46}$$

$$\lambda^2\gamma_0 = -\frac{2\lambda^2}{\lambda^2-1} - \frac{\lambda^3}{[\lambda^2-1]^{3/2}} \ln\left(\frac{\lambda-\sqrt{\lambda^2-1}}{\lambda+\sqrt{\lambda^2-1}}\right) \tag{47}$$

Inserting moments of inertia (38) - (39) and torques (40) - (42) into the equations of motion (35) - (37) and nondimensionalizing we obtain the governing equations for the rotational motion of ellipsoidal particles:

$$\frac{d\omega_{x'}}{dt} = \omega_{y'}\omega_{z'}\frac{\lambda^2-1}{1+\lambda^2} + \frac{20\nu}{a^2[\beta_0+\lambda^2\gamma_0]}\frac{\rho_f}{\rho_p}\frac{L}{u_0}\left[\frac{1-\lambda^2}{1+\lambda^2}f' + [\xi' - \omega_{x'}]\right] \tag{48}$$

$$\frac{d\omega_{y'}}{dt} = \omega_{z'}\omega_{x'}\frac{1-\lambda^2}{1+\lambda^2} + \frac{20\nu}{a^2[\alpha_0+\lambda^2\gamma_0]}\frac{\rho_f}{\rho_p}\frac{L}{u_0}\left[\frac{\lambda^2-1}{1+\lambda^2}g' + [\eta' - \omega_{y'}]\right] \tag{49}$$

$$\frac{d\omega_{z'}}{dt} = \frac{20\nu}{a^2[\alpha_0+\beta_0]}\frac{\rho_f}{\rho_p}\frac{L}{u_0}[\chi' - \omega_{z'}] \tag{50}$$

Kinematics

The translational displacement of the particle is linked to its velocity,

$$\frac{d\mathbf{r}}{dt} = \mathbf{v}. \tag{51}$$

In the rotational part of the kinematics, the time evolution of the Euler parameters is related to the angular velocity of the particle in the particle frame of reference, $\omega_{i'}$, and is given by

$$\frac{de_0}{dt} = \frac{1}{2}[-e_1\omega_{x'} - e_2\omega_{y'} - e_3\omega_{z'}] \tag{52}$$

$$\frac{de_1}{dt} = \frac{1}{2}[\;\; e_0\omega_{x'} - e_3\omega_{y'} + e_2\omega_{z'}] \tag{53}$$

$$\frac{de_2}{dt} = \frac{1}{2}[\;\; e_3\omega_{x'} + e_0\omega_{y'} - e_1\omega_{z'}] \tag{54}$$

$$\frac{de_3}{dt} = \frac{1}{2}[-e_2\omega_{x'} + e_1\omega_{y'} + e_0\omega_{z'}] \tag{55}$$

Numerical solution of the momentum equations (9), (34), (48) - (50) and kinematics equations (51)-(55) is needed in order to obtain the time evolution of the particle trajectories, and the backward Euler method is applied for numerical integration of equations.

3 Validation - particle transport in Couette and lid-driven cavity flows

The developed Lagrangian particle tracking model is validated for two well-known fluid benchmark test cases in order to understand the reliability and accuracy of the above models for ellipsoidal particles. The first numerical validation is performed for the case of Couette flow by comparing the present model results with results for spheres as well as Harper and Chang's lift model [12] results. Moreover, in order to validate the developed models for the case of a complex fluid flow, the results are compared to the experimental results by Tsorng et al. [29], who studied particle motion in a lid-driven cavity flow.

3.1 Simulation setup

All fluid flows in this numerical simulations are assumed to be stationary, and the particle influence on the fluid flow is neglected, leading to a one-way coupling of the fluid and particles. Due to low Reynolds number values the flow is considered laminar. The models considered for the kinematics and dynamics of the motion of ellipsoidal particles as summarized in section 2.3.2 are also used for the case of a spherical particle by setting the aspect ratio to one. Additional numerical models for spherical particles used for the numerical validation are introduced later in this section.

As the fluid-particle coupling is considered as a one-way coupling, prior to the Lagrangian particle tracking, numerical computation of the stationary flow fields (see Figure 1), i.e. Couette and lid-driven cavity flow, is conducted using the open-source code OpenFOAM® [30]. The cubic domain for both flow conditions is identical with the same edge length: $L = 0.1\,m$. For the lid-driven cavity case, the flow conditions are the same as used in the experimental study of Tsorng et al. [29]. The upper wall is moving with a constant velocity of $U_0 = 0.0813\,m/s$ in order to induce the shear flow in the cavity, with the resulting value of the Reynolds number $Re = \mu U_0/L = 470$. For lid-driven cavity flow at all other faces the non-slip boundary conditions are applied; for the Couette flow case, the zero gradient boundary conditions are assigned at the inlet and outlet boundaries whereas at the front and the back faces the symmetry boundary conditions are prescribed. For convenience, all boundary conditions are summarized in Table 1. The domain discretization consists of $40 \times 40 \times 40$ cells as shown in Figure 2, and several prism layers are adapted

in the near wall regions. The fluid flow regime in both cases is laminar, so no turbulence model is included in the computation. The specific fluid flow solver within the OpenFOAM® distribution used is the icoFoam, which solves the incompressible laminar Navier-Stokes equations using the PISO (pressure implicit with splitting of the operator) algorithm (Ferziger and Peric [9]). The particle Stokes number considered in the present study is 0.023, and the kinematic viscosity of the fluid is $17.3\,mm^2/s$.

Boundaries	Left & Right	Top & Bottom	Front & Back
Couette Flow	Zero Gradient	Non-slip	Full-slip
Lid-driven Cavity Flow	Non-slip	Non-slip	Non-slip

Table 1 Boundary conditions for Couette and lid-driven cavity flows.

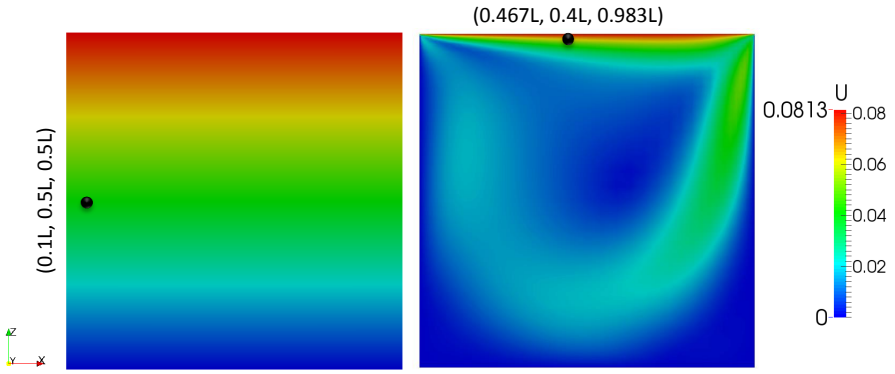

Fig. 1 Lagrangian particle tracking in Couette flow (left) and lid-driven cavity flow (right). Only one particle (black sphere) is placed in a predefined position: $x = 0.1L$, $y = 0.5L$, $z = 0.5L$ for Couette flow; $x = 0.467L$, $y = 0.4L$, $z = 0.983L$ for lid-driven cavity flow. For all cases: $Re = 470$, $D_{volume} = 3mm$, $[\rho_f - \rho_p]/\rho_f = 0.05\%$ or -0.07%, $St = 0.023$.

The spherical macro-particles used in Tsorng et al. [29] were plastic beads of diameter $D_p = 3\,mm$ and density $\rho_p = 1210\,kg/m^3$. For ellipsoidal particles, the volume equivalent diameter D_{volume} is considered. The relative density difference between the fluid and the particle, i.e. $[\rho_f - \rho_p]/\rho_f$, is very small, i.e. about 0.05% or –0.07%, indicating slightly positive or negative buoyancy conditions. The relative density difference cannot be set too large, otherwise, a particle does not predominantly follow the flow and can easily hit the wall, thus creating an additional problem in specifying correct experimental data. In the numerical simulation, only a single particle is placed in the fluid domain with applied rotation of the major axis

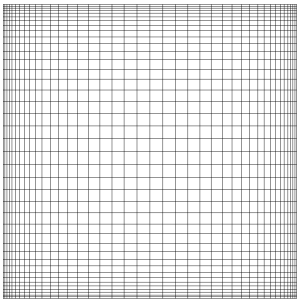

Fig. 2 Computational grid for the fluid domain; resolution: $40 \times 40 \times 40$ grid cells.

b in the direction perpendicular to the stream-wise direction (i.e. x-direction). As illustrated in Figure 1, the initial position of the particle in lid-driven cavity flow is at $[0.467L, 0.4L, 0.983L]$, and at $[0.1L, 0.5L, 0.5L]$ in the case of Couette flow.

The verification of drag and lift forces in linear shear flow and torques acting on non-spherical particles by the developed models was already demonstrated by Brenner [2], Fan and Ahmadi [6], Harper and Chang [12], Hogg [13] and Jeffery [16]. In order to demonstrate the accuracy of the new model for the shear lift force (Eq. 34), several models for spheres were chosen to compare with (Sommerfeld and Schmalfuss [27]). These models are widely used for Lagrangian particle tracking at higher particle Reynolds numbers including the drag force, the transverse lift force due to shear flow and particle rotation, as well as in particle rotation models, with more details in Sommerfeld and Schmalfuss [27]. Finally, all developed particle models are implemented into the Lagrangian solver icoUncoupledKinematicParcelFoam, a transient solver for the passive transport of a single kinematic particle cloud, included in the OpenFOAM®, which is finally used for Lagrangian particle tracking computations.

3.2 Couette flow

The numerical accuracy of the proposed model for ellipsoidal particles is studied in this section by comparing them with other numerical models for spherical particles [27] as well as ellipsoidal particles [12]. In Couette flow a particle moves due to the drag force in the stream-wise direction, and is lifted by the linear shear $\partial u_x/\partial z$. In the following results, we use Sommerfeld et al. to denote numerical models for spherical particles [27]. The effect of gravity was neglected in the simulation, while drag and shear lift force were calculated either jointly or separately.

The time evolution of a sphere, with its initial relative velocity between the fluid and the particle equal to zero, i.e. $\mathbf{u}_0 - \mathbf{v}_0 = \mathbf{0}\,m/s$, under the action of different drag forces, is indicated by black and red lines and is plotted in Figure 3. It should be

noted that the initial relative velocity in the stream-wise direction is not exactly zero due to numerical errors. Therefore a small drag force, about $2.66nN$, is observed at the beginning and is reduced afterwards as the particle approaches the velocity of the flow. After 0.2 seconds a quasi-steady state is reached since the particle is accelerated and decelerated by the flow due to the small density difference, i.e. $[\rho_f - \rho_p]/\rho_f = -0.07\%$. The overlapping of the results shows that our drag model demonstrates good agreement with the results of Sommerfeld et al. for the case of spherical particles. When the initial relative velocity is increased to match the velocity of the fluid (i.e. $\mathbf{v}_0 = \mathbf{0}m/s$), the difference in the results between the present work and Sommerfeld et al. (i.e. blue and magenta lines in Figure 3) becomes evident. The reason for the difference in the results is due to the fact that in the case of larger relative velocities the Stokes flow conditions in the vicinity of the particle (i.e. creeping flow, relative velocity close to zero) are no longer satisfied. Sommerfeld et al. [27] accounted for this effect by implementing an additional term solving the drag problem at high relative velocities and high Stokes numbers, where particles do not predominantly follow the fluid streamlines. Therefore, the simulations considering the influence of the drag force on ellipsoidal particles are performed only with small relative velocity.

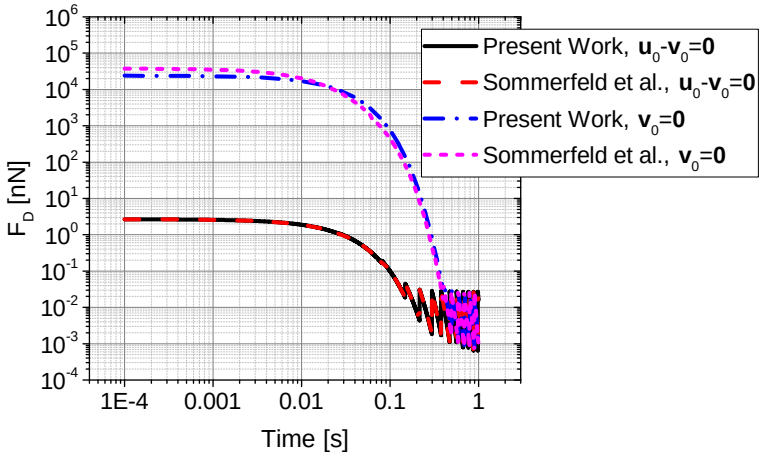

Fig. 3 Time evolution of the drag force on a spherical particle in Couette flow in comparison to alternative drag force models and initial relative velocities ($Time = 1s$, $\lambda = 1$, $D_p = 3mm$, $Re = 470$, $L = 0.1m$, $[\rho_f - \rho_p]/\rho_f = -0.07\%$).

The Couette flow considered here (i.e. linear shear flow, Figure 1) with shear rate $\partial u_x/\partial z$ shares the same characteristics of the shear lift force of Harper and Chang (Eq. 26), so the new shear lift force (Eq. 34) can be compared to the results of Harper and Chang for different aspect ratios, as shown in Figure 4. These simulations are only performed for test purposes by switching on the shear lift force and turning off the drag force, in order to eliminate the influence of the drag on the translational

movement of the particle. Moreover, the initial velocity of the particle is set to zero for the purpose of increasing the shear lift force in the vertical direction. The ellipsoid is initially placed with its major axis b perpendicular to the flow direction. The new model results are in good agreement with the results of Harper and Chang for all aspect ratios. This is obvious since the new model is identical to Harper and Chang's model in a linear shear flow (Eq. 26 and 34). Furthermore, the particle travels a shorter distance in the vertical direction (z-direction) at larger aspect ratios, since the cross-sectional area of the minor axis a is reduced at the same volume equivalent diameter D_{volume}, which leads to a decrease of the shear lift force in the vertical direction.

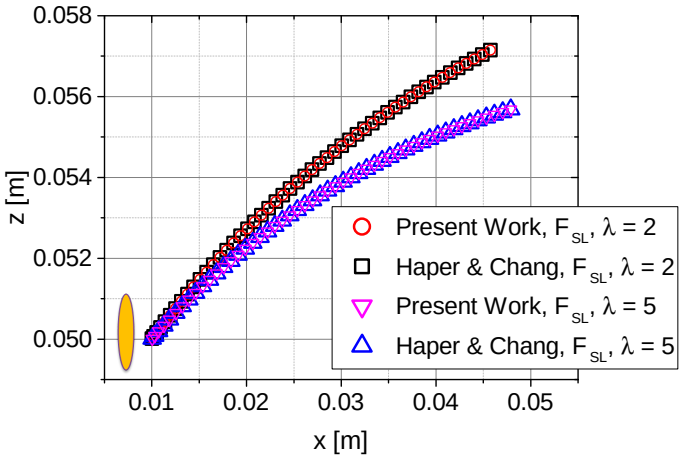

Fig. 4 Translational motion of an ellipsoidal particle in Couette flow for different aspect ratios; a comparison of various shear lift forces; the initial velocity of the particle is set to zero ($\mathbf{v}_0 = \mathbf{0}\,m/s$, $Time = 1\,s$, $\lambda = 1$, $D_p = 3\,mm$, $Re = 470$, $L = 0.1\,m$, $[\rho_f - \rho_p]/\rho_f = -0.07\%$).

After the validation of the new lift force, a parameter study is performed. In this study, both the drag and the generalized shear lift forces are incorporated in the simulation. The initial velocity of the particle relative to the fluid is set to zero. Figure 5a plots the time evolution of the drag force in the stream-line and vertical directions (i.e. x and z-directions) for different aspect ratio values. The component of the drag force in the stream-line direction is largest at the beginning of the simulation, about $2.9\,nN$ to $4.7\,nN$, and increases with increasing the aspect ratio λ from 2 to 10. Although the initial condition of zero relative velocity between the particle and the fluid (Eq. 33) was chosen, due to numerical errors in computing the x-component of the relative velocity, a non-zero drag force is computed. As a consequence of the decrease in relative velocity and the rotation of the particle, the drag force decreases significantly after only $0.1\,s$. The ellipsoidal particle tends to align its major axis b with the direction in which it is subject to a minimum torque, i.e. the mean flow direction in the linear shear flow, resulting in a decrease of the exposed cross-

sectional area and hence reduction of the drag. Figure 5b shows a close-up of the drag force components in the time period from $0.2\,s$ to $1.0\,s$. The vertical component of the drag force assumes negative values, as the particle moves in the upward direction due to the shear lift, resulting in negative relative velocity in the z-direction and hence negative drag force. When the flow resistance stabilizes i.e. after $0.6\,s$, the x-component of the drag force fluctuates only slightly due to the creeping flow condition. The magnitude of the z-component of the drag increases with increasing aspect ratios since the exposed cross-sectional area of the ellipsoidal particle in the z direction becomes larger, which is a consequence of the geometry of the particle.

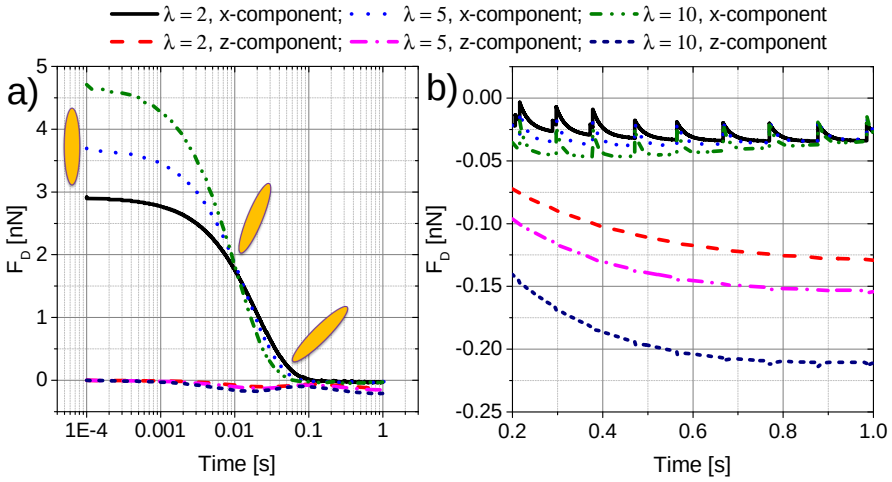

Fig. 5 Time evolution of x and z-components of the drag force acting on an ellipsoidal particle in Couette flow for different aspect ratios; simulation with drag and shear lift force for ellipsoidal particles; the initial velocity of the particle relative to the fluid is set to zero; a) whole time period; b) time period between $0.2\,s$ and $1\,s$ ($\mathbf{u}_0 - \mathbf{v}_0 = \mathbf{0}\,m/s$, $Time = 1\,s$, $D_{volume} = 3\,mm$, $Re = 470$, $L = 0.1\,m$, $[\rho_f - \rho_p]/\rho_f = -0.07\%$).

The corresponding generalized shear lift force in the stream-line and vertical directions are presented in Figure 6. The largest shear lift force of the ellipsoid in the range of $1.0\,nN$ to $2.7\,nN$ is observed at the beginning of the simulation. Afterwards, the shear lift force decreases as the particle is accelerated or decelerated by the drag and more closely follows the flow. This leads to a decrease in relative velocity between the particle and the fluid. After $0.2\,s$, the x-components of the shear lift force for different aspect ratios become very small, in the range $0.038\,nN - 0.04\,nN$ at $1.0\,s$, whereas the z-components are relatively large, in the range $0.13\,nN - 0.21\,nN$ at $1.0\,s$, and increase with increasing aspect ratios. The difference between the x and z-components of the drag and shear lift forces are mainly a consequence of the difference in relative velocity between the particle and the fluid. When the particle becomes more or less stable, i.e. after $0.6\,s$, the magnitude of the relative velocity in the stream-line direction becomes very small as the velocities in the flow direction

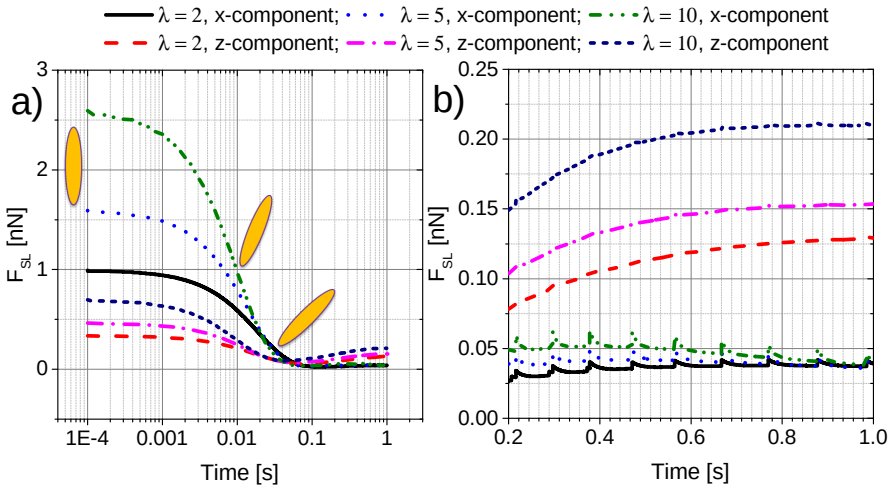

Fig. 6 Time evolution of x and z-components of the shear lift force on an ellipsoidal particle in Couette flow for different aspect ratios; simulation with drag and shear lift force for ellipsoidal particles; the initial velocity of the particle relative to the fluid is set to zero; a) whole time period; b) time period between $0.2\,s$ and $1\,s$ ($\mathbf{u}_0 - \mathbf{v}_0 = \mathbf{0}\,m/s$, $Time = 1\,s$, $D_{volume} = 3\,mm$, $Re = 470$, $L = 0.1\,m$, $[\rho_f - \rho_p]/\rho_f = -0.07\%$).

are constant, while in the vertical direction it is much larger due to the existence of the shear rate $\partial u_x/\partial z$. Therefore, both the drag and the shear lift forces in the flow direction are smaller than force magnitudes observed in the vertical direction.

3.3 Lid-driven cavity flow

The lid-driven cavity is a well-known benchmark problem for viscous incompressible fluid flows and has been studied extensively using analytical approaches (Shankar and Deshpande [25]), in laboratory experiments (Koseff and Street [17], Tsorng et al. [29]) and through numerical investigations (Chiang and Sheu [3]). However, research on the motion of particles in lid-driven cavity flows is relatively sparse. Tsorng et al. [29] investigated the behaviour of macroscopic rigid particles suspended in a fully three-dimensional viscous flow in a closed cubic cavity. The motion of macro sized spherical particles in the approximate plane $y/L \approx 0.4$ near the upper downstream corner of the cavity was determined based on data from video images. The fluid streamlines computed from the numerical simulation are presented in Figure 7. At $Re = 470$, the flow pattern is driven by the moving top lid, generating a large primary eddy which occupies most of the cavity (Figure 7a), and two secondary eddies form at the lower downstream corner in the transverse plane (Figure 7b). The longitudinal plane $y/L \approx 0.4$ (red line in Figure 7b) was chosen

for the particle tracking because it features at its upper downstream corner an open pathway linking the primary eddy to the downstream secondary eddy [29].

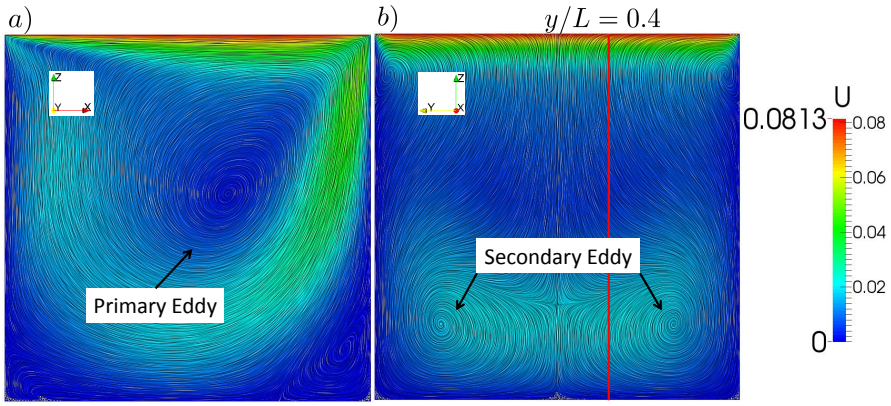

Fig. 7 Numerically calculated fluid streamlines in a lid-driven cavity flow; a) the central longitudinal plane $y/L = 0.4$; b) the central transverse plane $x/L = 0.5$; the red line indicate the plane of particle tracking $y/L = 0.4$; U is the magnitude of the fluid velocity ($\mathbf{u}_0 - \mathbf{v}_0 = \mathbf{0}\,m/s$, $Time = 5\,s$, $\lambda = 1$, $D_p = 3\,mm$, $Re = 470$, $L = 0.1\,m$, $[\rho_f - \rho_p]/\rho_f = 0.05\%$).

The trajectories of the tracked spherical particle from experimental measurements (square symbols) and numerical calculations (colour lines) are presented in Figure 8. The forces considered in the simulations are drag, gravity, lift force due to the shear flow and due to relative rotation. The Brenner's drag force is applicable to both spheres and ellipsoids whereas the generalized shear lift force is used for the calculation of ellipsoidal particles. Hence only the Brenner's drag is compared to other models for spheres [27]. As shown in Figure 8, the results of different combinations of forces are nearly the same, which implies that the influence of the drag force is much larger than the lift force and dominates the translational motion of spherical particles. When the relative density difference increases, the sphere travels a shorter distance due to the change from negative to positive buoyancy conditions. Moreover, a slight difference is found between the present work and Sommerfeld et al. under the condition of $F_D + G$. The reason is that the Stokes flow condition is not satisfied in the upper downstream corner of the cavity since the particle changes its direction and moves downward. Additionally, the numerical results also show a good agreement with experimental data of Tsorng et al. [29], with a minor difference arising from the finite size effect of the macro-sized particles, i.e. $3\,mm$, whereas in our Lagrangian particle tracking the point particle assumption was adopted.

Figure 9a plots the trajectories of the tracked ellipsoidal particles over a time period of $5\,s$ under the condition of $F_D + G$. With increasing aspect ratios, the ellipsoidal particle tends to move away from the right side wall. This can be explained by Figure 9b, which shows the drag force as a function of time for a period of $5\,s$ at different aspect ratios. The drag forces initially decrease since the particle tends to

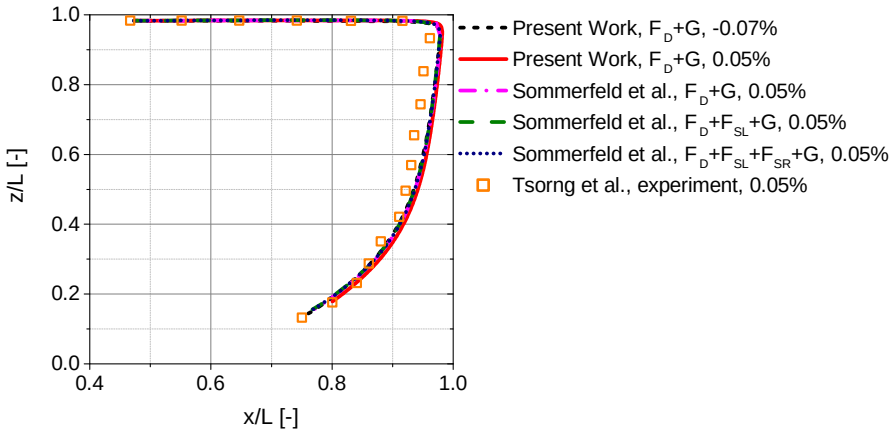

Fig. 8 Translational motion of a spherical particle in a lid-driven cavity flow obtained from both numerical and experimental studies ($\mathbf{u}_0 - \mathbf{v}_0 = \mathbf{0}\,m/s$, $Time = 5\,s$, $D_p = 3\,mm$, $Re = 470$, $L = 0.1\,m$, $[\rho_f - \rho_p]/\rho_f = 0.05\%$ or -0.07%).

align its major axis b with the direction which subjects the particle to the minimum torque (i.e. mean flow direction before entering the upper downstream corner). Subsequently, the drag force increases significantly as the particle approaches the upper downstream corner where the ellipsoidal particle rotates and the relative velocity increases. After that, the particle aligns its major axis with the mean flow direction again, and hence the drag force is drastically reduced. At higher aspect ratio, i.e. $\lambda = 5$, the particle experiences smaller drag force after escaping from the upper downstream corner (see Figure 9b time period $3.5\,s$ to $5.0\,s$), therefore the direction of the particle is slightly changed and as a result the particle moves away from the right side wall.

The existence of the shear lift force has a significant influence on the translational motion of ellipsoidal particles in cavity flows as illustrated in Figure 10a. The lid is the moving wall and the fluid nearby has the highest velocity. Therefore, the particle is lifted by the shear and moves closer to the top wall. Eventually, the particle enters the upper downstream region where the fluid vorticity is very large. The particle picks up spin due to higher vorticity of the fluid flow and becomes almost stationary. It remains in the upper right corner of the cavity for an extended duration of time. This phenomenon is also captured by the time evolution of the drag and lift forces as shown in Figure 10b. In the beginning, i.e. $0\,s$ to $0.7\,s$, the drag force rises due to the increase in fluid velocity, as the particle is moving upwards due to the lift force. The lift force decreases because the cross-sectional area exposed to the fluid flow is smaller. After some time in the downstream region, due to the particle rotation, the particle eventually becomes increasingly unstable which results in higher drag and lift forces. After having found a new stable position at $3.9\,s$, the reorientation dynamics of the particle are reduced leading to a decrease in drag and shear lift forces. This is followed by a subsequent increase in drag and shear lift force due

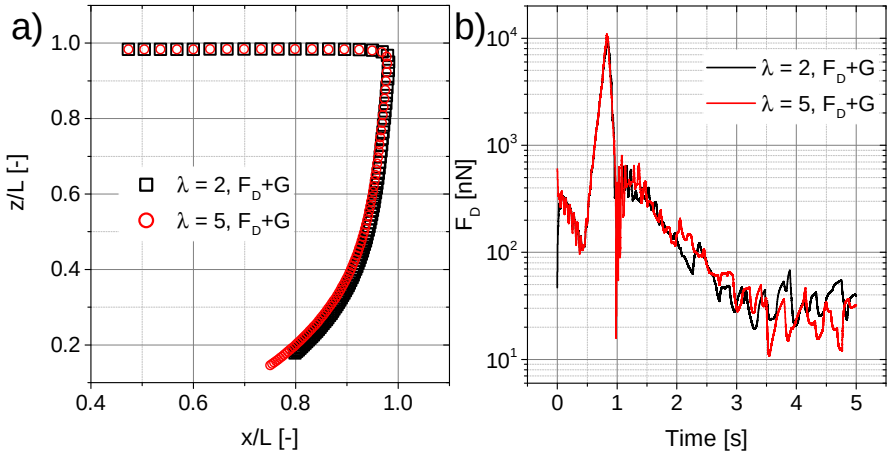

Fig. 9 The influence of the drag force on the translational motion of an ellipsoidal particle in a lid-driven cavity flow for different aspect ratios; a) translational motion of the ellipsoid in the cavity; b) time evolution of the drag force on the ellipsoid; for all cases only the drag force and the gravity were take into account ($\mathbf{u}_0 - \mathbf{v}_0 = \mathbf{0} m/s$, $Time = 5\,s$, $D_{volume} = 3\,mm$, $Re = 470$, $L = 0.1\,m$, $[\rho_f - \rho_p]/\rho_f = 0.05\%$).

to the particle changing the spin direction from clock-wise to counter clock-wise. Eventually, the ellipsoidal particle moves out of the top right corner and aligns its major axis b with the mean flow direction, hence reducing the drag force.

4 Conclusions

Numerical simulation of non-spherical particle transport in complex fluid dominated flows still presents a research challenge, as the established models of fluid-particle interaction are predominantly valid only for spherical particles. In the case of momentum transport from fluid flow to non-spherical solid particles, the effect of the orientation of a particle must not be neglected. An ellipsoidal particle is a good example of a non-spherical particle, that is frequently encountered in technical or biological systems.

In the present paper, a Lagrangian particle tracking algorithm for simulating the motion of particles of ellipsoid shape was developed within the open-source code OpenFOAM®. The main objective of the present study is the evaluation of the drag and the lift forces with respect to the orientation of ellipsoidal particles. Instead of the Euler angles parametrization of the rotation tensor in Euler parameters/quaternions is used in order to avoid singularity issues. The rotation tensor provides the essential connection between the inertial frame and the particle rotational frame of reference. The time evolution of the Euler parameters is related to

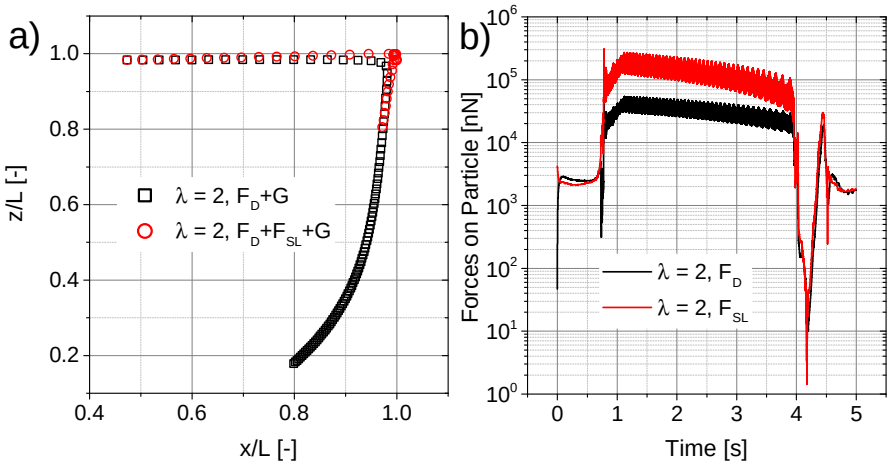

Fig. 10 The influence of the generalized shear lift force on the translational motion of an ellipsoidal particle in a lid-driven cavity flow; a) translational motion of the ellipsoid in the cavity in comparison to two different force combinations, i.e. $F_D + G$ and $F_D + F_{SL} + G$; b) time evolution of the drag force and generalized shear lift forces on the ellipsoid under the condition of $F_D + F_{SL} + G$; $(\mathbf{u}_0 - \mathbf{v}_0 = \mathbf{0}\, m/s, Time = 5\, s, \lambda = 2, D_{volume} = 3\, mm, Re = 470, L = 0.1\, m, [\rho_f - \rho_p]/\rho_f = 0.05\%)$.

the orientation angular velocity of ellipsoidal particles, resulting from rotational dynamics, whereas for the resistance to rotational motion the linear Jeffery torque [16] was adopted. In order to account for the effect of the particle shape, in modeling the drag force and the shear lift force exerted on an ellipsoidal particle the resistance tensor and the lift tensor, had to be implemented. The resistance tensor was used in the form developed by Brenner [1], who introduced a resistance tensor based on the aspect ratio of the ellipsoid and implemented it for computation of the hydrodynamic drag force acting on an ellipsoidal particle under Stokes flow conditions. The main achievement of the present paper is the derivation of a general lift vector, based on permutations of the linear shear lift tensor, that can be used in the computation of the shear lift force for a general shear flow.

In order to understand the accuracy and reliability of the overall model for Lagrangian tracking of ellipsoidal particles, numerical and experimental validations were performed for Couette and lid-driven cavity flows. First, the drag force was validated with numerical models for spheres (Sommerfeld et al. [27]) and the new shear lift forces was validated with a numerical model for ellipsoids (Harper and Chang [12]) in Couette flow, showing good agreement of the results under Stokes flow conditions. Secondly, the influence of drag and shear lift forces with respect to the particle orientation was studied for various ellipsoid aspect ratio values. With the main axis perpendicular to the incoming flow direction, the ellipsoidal particle starts to rotate due to the shear and tends to align its major axis with the mean flow direction, resulting in a decrease of the drag and shear lift forces in the mean flow direction and an increase of both forces in the vertical direction. As a second test case,

results of numerical models were compared with experimental investigations of particle transport in a lid-driven cavity flow (Tsorng et al. [29]). In general, the present model for ellipsoidal particles shows good agreement with the numerical and experimental results. In the case of an ellipsoidal particle, the shear lift force plays an important role in the translational motion of the particle. The ellipsoid moves closer to the lid and enters the upper downstream corner of the cavity, where its residence time is larger than in the case of the spherical particle.

The presented contribution to the further development of the classical Lagrangian particle tracking model was focused on the generalization of the shear lift force model for ellipsoids to a general shear flow. The model gives accurate results under the conditions of Stokes flow around the particle and can, therefore, be used in the numerical computation of fluid dominated particle transport problems. In order to extend the applicability of the derived model, the future work will focus on the dynamics of particle rotation by developing models taking into account the finite-size effect of the particles.

Acknowledgements The authors thank the Deutsche Forschungsgemeinschaft for the financial support in the framework of the project STE 544/58.

References

1. H Brenner. The Stokes resistance of an arbitrary particle. *Chem. Eng. Sci*, 18:1–25, 1963.
2. H Brenner. The Stokes resistance of an arbitrary particle - IV. Arbitrary fields of flow. *Chem. Eng. Sci*, 19:703–727, 1964.
3. T P Chiang and W H Sheu. Numerical prediction of eddy structure in a shear-driven cavity. *Computational Mechanics*, 20(4):379–396, 1997.
4. C T Crowe, M Sommerfeld, and Y Tsuji. *Multiphase flows with droplets and particles*. CRC press, 1998.
5. J J Derksen. Numerical Simulation of Solids Suspension in a Stirred Tank. *AIChE Journal*, 49:2700–2714, 2003.
6. F Fan and G Ahmadi. A sublayer model for wall deposition of ellipsoidal particles in turbulent streams. *J. Aerosol Sci.*, 26:813–840, 1995.
7. M Fantoni. *Dynamics of ellipsiodal particles dispersed in channel flow turbulence*. PhD thesis, University of Udine, 2008.
8. Y. Feng and C. Kleinstreuer. Analysis of non-spherical particle transport in complex internal shear flows. *Physics of Fluids*, 25(9):091904, 2013.
9. J.H. Ferziger and M. Peric. *Computational Methods for Fluid Dynamics*. Springer, 3rd edition, 2002.
10. I Gallily and A.-H. Cohen. On the orderly nature of the motion of nonspherical aerosol particles II. Inertial collision between a spherical large droplet and axially symmetrical elongated particle. *J. Colloid Interface Sci.*, 68:338–356, 1979.
11. H Goldstein. *Classical Mechanics, 2nd Edition*. Addison Wesely, Reading MA., 1980.
12. E Y Harper and I-Dee Chang. Maximum dissipation resulting from lift in a slow viscous shear flow. *Journal of Fluid Mechanics*, 33(02):209–225, aug 1968.
13. A J Hogg. The inertial migration of non-neutrally buoyant spherical particles in two-dimensional shear flows. *J. Fluid Mech.*, 212:285–318, 1994.
14. M. Hriberšek, B. Žajdela, A. Hribernik, and M. Zadravec. Experimental and numerical investigations of sedimentation of porous wastewater sludge flocs. *Water Research*, 45(4):1729–1735, 2011.

15. A Jafari, T Tynjälä, S M Mousavi, and P Sarkomaa. Simulation of heat transfer in a ferrofluid using computational fluid dynamics technique. *International Journal of Heat and Fluid Flow*, 29:1197–1202, 2008.
16. G B Jeffery. The motion of ellipsoidal particles immersed in a viscous fluid. *Proc. R. Soc. A*, 102:161–179, 1922.
17. J R Koseff and R L Street. The lid-driven cavity flow: a synthesis of qualitative and quantitative observations. *J. Fluids Eng.*, 106:385–389, 1984.
18. C Marchioli, M Fantoni, and A Soldati. Orientation, distribution and deposition of elongated, inertial fibers in turbulent channel flow. *Phys. Fluids*, 49:33301, 2010.
19. Martin R Maxey. Equation of motion for a small rigid sphere in a nonuniform flow. *Physics of Fluids*, 26(4):883, 1983.
20. M.Sommerfeld. *Modellierung und numerische Berechnung von partikelbeladenen turbulenten Strömungen mit Hilfe des Euler/Lagrange- Verfahrens*. Shaker Verlag, Aachen, 1996.
21. J. Ravnik and M. Hriberšek. High gradient magnetic particle separation in viscous flows by 3D BEM. *Computational Mechanics*, 51(4):465–474, 2012.
22. J Ravnik, C Marchioli, M Hriberšek, and A Soldati. On shear lift force modelling for non-spherical particles in turbulent flows. In G Psihoyios T. E. Simos and Ch. Tsitouras, editors, *AIP Conference Proceedings*, volume 1558, pages 1107–1110, Rhodes, Greece, 2013.
23. P G Saffman. The lift on a small sphere in a slow shear flow. *J. Fluid Mech.*, 22:385, 1965.
24. P G Saffman. Corrigendum to: The lift on a small sphere in a slow shear flow. *J. Fluid Mech.*, 31:624, 1968.
25. P N Shankar and M D Deshpande. Fluid mechanics in the driven cavity. *Annu. Re. Fluid. Mech.*, 32:93–136, 2000.
26. M Shapiro and M Goldenberg. Deposition of glass fiber particles from turbulent air flow in a pipe. *J. Aerosol Sci.*, 24:65–87, 1993.
27. M. Sommerfeld and S. Schmalfuss. Numerical Analysis of Carrier Particle Motion in a Dry Powder Inhaler. *ASME Journal of Fluids Engineering*, 138, 2015.
28. H A Stone. Philip Saffman and viscous flow theory. *J. Fluid Mech.*, 409:165–183, 2000.
29. S J Tsorng, H Capart, D C Lo, J S Lai, and D L Young. Behaviour of macroscopic rigid spheres in lid-driven cavity flow. *Int. J. Multiphase Flow*, 34:76–101, 2008.
30. H G Weller, G Tabor, H Jasak, and C Fureby. A tensorial approach to computational continuum mechanics using object-oriented techniques. *Computers in Physics*, 12(6):620–631, 1998.
31. M Zadravec, M. Hriberšek, P Steinmann, and J Ravnik. High gradient magnetic particle separation in a channel with bifurcations. *Engineering Analysis with Boundary Elements*, 49(0):22–30, 2014.